Cancer-Related Axonogenesis and Neurogenesis in Prostate Cancer

Gustavo E. Ayala,[1,2] Hong Dai,[1] Michael Powell,[1] Rile Li,[1] Yi Ding,[1] Thomas M. Wheeler,[1,2] David Shine,[4] Dov Kadmon,[2] Timothy Thompson,[5] Brian J. Miles,[2] Michael M. Ittmann,[1] and David Rowley[3]

Abstract

Purpose: Perineural invasion is the only interaction between cancer cells and nerves studied to date. It is a symbiotic relationship between cancer and nerves that results in growth advantage for both. In this article, we present data on a novel biological phenomenon, cancer-related axonogenesis and neurogenesis.

Experimental Design: We identify spatial and temporal associations between increased nerve density and preneoplastic and neoplastic lesions of the human prostate.

Results: Nerve density was increased in cancer areas as well as in preneoplastic lesions compared with controls. Two- and three-dimensional reconstructions of entire prostates confirmed axonogenesis in human tumors. Furthermore, patients with prostate cancer had increased numbers of neurons in their prostatic ganglia compared with controls, corroborating neurogenesis. Finally, two *in vitro* models confirmed that cancer cells, particularly when interacting with nerves in perineural invasion, induce neurite outgrowth in prostate cancer. Neurogenesis is correlated with features of aggressive prostate cancer and with recurrence in prostate cancer. We also present a putative regulatory mechanism based on semaphorin 4F (S4F). S4F is overexpressed in cancers cells in the perineural *in vitro* model. Overexpression of S4F in prostate cancer cells induces neurogenesis in the N1E-115 neurogenesis assay and S4F inhibition by small interfering RNA blocks this effect.

Conclusions: This is the first description of cancer-related neurogenesis and its putative regulatory mechanism.

Nerves play a fundamental role not only in the biology of prostate cancer but also in the normal prostate epithelium. The prostate is thoroughly innervated and receives autonomic innervation through the hypogastric and pelvic nerves (1). Our studies of prostate nerve density in a group of cancer-free patients have shown that nerve density of the peripheral zone, where prostate cancer is more frequent, is significantly greater than that of the transition zone. Both overall nerve density and peripheral zone nerve density decrease with increasing age.

Nerves have numerous interactions with the epithelial and stromal components of the prostate. Nerves are involved in prostate development and maintenance of the adult phenotype. Several reports have shown that mechanical and/or chemical denervation of the pelvic plexus of Sprague-Dawley and Wistar rats and dogs causes morphologic and functional changes in the prostate (2–6). Denervated prostates have an overall decrease in cell height and secretory reduction (3). In humans and rats, the embryologic formation of the prostate requires intact innervation. Maturation of the prostate during adolescence also requires the presence of nerves. These findings strongly suggest that prostate function not only is regulated by androgens but also is subject to the trophic influences of nerves (5, 7, 8).

The best-known interaction between nerves and cancer in prostate cancer is perineural invasion (PNI), the process by which cancer cells invade around nerves (9). It is seen most frequently in certain types of cancer such as prostate, bile duct, and pancreatic carcinomas as well as in head and neck cancers. These cancers are known as "neurotropic cancers." PNI is a common phenomenon in prostate cancer and is believed to be responsible for most extracapsular spread of prostate cancer (1). Mechanisms that directly underlie PNI are now better understood through our studies using an *in vitro* model of PNI, suggesting that PNI is an interactive process between nerves and cancer cells (10). In this model, specific interactions between prostate cancer cells and nerves lead to costimulation of growth. PNI provides microenvironmental factors that result in increased survival advantage for cancer cells in the perineural space. Prostate cancer cells in PNI exhibited a significantly reduced rate of apoptosis and an increased rate of proliferation both *in vitro* and in human tissues. Furthermore, our observations show that two mechanisms might be involved in this survival advantage: (*a*) an epithelial pathway based on up-regulation of nuclear factor-κB and its downstream targets PIM-2 and DAD-1 and (*b*) a stromal pathway based on secretion of caveolin-1 in the perineural space (11). The significance of nerves in prostate cancer is further substantiated

Authors' Affiliations: Departments of [1]Pathology, [2]Urology, [3]Molecular and Cellular Biology, and [4]Neurosurgery, Baylor College of Medicine, and [5]Genitourinary Medical Oncology – Research, M. D. Anderson Cancer Center, Houston, Texas.

Received 5/9/08; revised 7/11/08; accepted 7/17/08.

Grant support: NIH grants SPORE P50 CA58204 and TMEN U54CA126568-01.

The costs of publication of this article were defrayed in part by the payment of page charges. This article must therefore be hereby marked *advertisement* in accordance with 18 U.S.C. Section 1734 solely to indicate this fact.

Note: Supplementary data for this article are available at Clinical Cancer Research Online (http://clincancerres.aacrjournals.org/).

Requests for reprints: Gustavo E. Ayala, Department of Pathology and Scott Department of Urology, Baylor College of Medicine, Houston, TX 77401. Phone: 713-798-3705; Fax: 713-444-9887; E-mail: gayala@bcm.tmc.edu.

doi:10.1158/1078-0432.CCR-08-1164

Translational Relevance

The major strength of this article is novelty, as this innovative biological occurrence has never been described. We present very strong evidence of axonogenesis and neurogenesis as a biological phenomenon. The two- and three-dimensional reconstructions of entire prostates are a major step in the confirmation of the process. As a benchmark, it took researchers years to accept angiogenesis as a three-dimensional true phenomenon. We also present mechanistic data on S4F. We believe that axonogenesis/neurogenesis not only is found in prostate cancer (data not presented) and but also is potentially a generalizable concept in cancer. It is our perception that other cancers use this mechanism as well, mostly the neurotrophic cancers. Furthermore, neurogenesis, in close regulatory connection with angiogenesis, is part of the wound repair response. The identification of cancer-related neurogenesis has momentous implications for carcinogenesis research and as a therapeutic target. You cannot target a phenomenon that is not known. We deem that it will probably open a new research field, as other investigators confirm and advance these findings, just as the original description of angiogenesis did. We hope that this original article will become a seminal article introducing the concept of cancer-related neurogenesis.

by the fact that spinal cord injury patients rarely develop prostate cancer (12, 13). Conversely, the PNI *in vitro* model also predicts that the cancer cells induce neurogenesis.

Semaphorins constitute the largest family of axon guidance cues yet described and are composed of at least 30 members in 8 different classes. They are characterized by the presence of ~500 amino acid NH_2-terminal semaphorin domain. Of the 8 classes, classes 3 to 7 are found in vertebrates, whereas classes 1 and 2 are found in invertebrates and class 8 is a viral semaphorin (14). Of the vertebrate classes, class 3 contains secreted semaphorins and classes 4 to 7 contain transmembrane or membrane-anchored semaphorins. Their receptors include members of the neuropilin and plexin families, but there is great redundancy in the formation of the receptor complexes (15). Semaphorins are classically described as collapsing factors and mediators of axon repulsion. However, they may act as context-dependent chemoattractants as well (16). Outside the nervous system, semaphorins also have putative roles in cardiovascular development and the immune response (17). M-sema H correlates with the metastatic ability of mouse tumor cell lines (18) and semaphorin E is a non-multidrug-resistant gene of human cancers (19).

The PNI *in vitro* model predicted increased nerve growth in the presence of prostate cancer cells (10). We now present data showing cancer-related axonogenesis and potentially even neurogenesis in human tissues. We will refer to axonogenesis as the enlargement of nerves or increase in nerve density (axon extension and increased number), whereas neurogenesis requires an increase in neuron body cell numbers. We present data that identify spatial and temporal associations between increased nerve density/increased neurons and preneoplastic/neoplastic lesions of the human prostate. We also present substantiating *in vitro* data. We show that this phenomenon is significant in human prostate cancer disease. Finally, we present a putative regulatory mechanism for cancer-related neurogenesis based on a member of the semaphorin family, semaphorin 4F (S4F).

Materials and Methods

In vitro studies

Tissue culture. Three cell lines were used in this experiment: DU145 human prostate cancer, N1E-115 mouse neuroblastoma, and PC-12 rat pheochromocytoma cell line, all obtained from the American Type Culture Collection. DU145 and N1E-115 were cultured in DMEM (Invitrogen) supplemented with 10% fetal bovine serum and 1% penicillin/streptomycin (Invitrogen). DU145 cells were incubated at 37°C in a 5% CO_2 atmosphere. N1E-115 cells were incubated at 37°C in a 10% CO_2 atmosphere.

Cancer/DRG coculture. Cancer cells were cultured alone as well as in tandem with mouse DRG (10). After 4 days, supernatant was collected from all wells and pooled by type and frozen at -80°C for later use.

PC-12 neurogenesis assay. Forty-eight hours before experimentation, PC-12 cells were induced to neurons following standard procedure. DU145 PNI *in vitro* coculture and controls were prepared. Individual membranes (Chemicon) attached to plastic inserts were incubated in collagen I solution (Chemicon) at 37°C for 2 h. After incubation, membranes were immersed in samples of supernatants from the PNI cocultures described above. After incubation, membranes were removed and rinsed in PBS and then fixed in ice-cold absolute methanol and placed in Chemicon Neurite Stain Solution. Stained membranes were rinsed in PBS and then cleaned using sterile cotton swabs to separate cell bodies from the neurites. The membranes were extracted and quantified by absorbance at 562 nm.

N1E-115 neurite outgrowth assay. N1E-115 cells were starved of serum for 48 h before experiment. After serum starvation, cells were harvested using Puck's Saline A (Sigma) supplemented with 58.4 mmol/L sucrose, 0.17 mmol/L dibasic sodium phosphate heptahydrate, and 0.22 mmol/L anhydrous monobasic potassium phosphate (Sigma). Harvested cells were centrifuged and resuspended in serum-free DMEM at a concentration of 200,000/mL. Each well of a six-well plate was seeded with 1.5 mL cell suspension and then supplemented with 1.5 mL previously frozen cancer/DRG coculture supernatant. Four samples of DU145/DRG coculture supernatant were seeded along with four samples of DU145 supernatant alone. Plates were incubated at 37°C in 10% CO_2. After 48 h, waste medium was aspirated to remove dead and floating cells, and fresh serum-free DMEM was added. Each well was photographed digitally four times with a Nikon camera at two random locations, a location of high cell concentration and a location of high neurite concentration. Images of the N1E-115 cells were analyzed using the Optimas 6 Image Analysis Suite. In each image, the following quantities were measured: number of neurites, number of cells, number of neurite sprouts or branching, and total neurite length. Based on these measurements, the following quantities could also be computed: neurites per cell and sprouts or branchings per cell.

Human tissue studies

Hotspot nerve density. In a retrospective case-controlled, age-matched study, we selected 27 radical prostatectomy patients with cancer. We selected only patients with large volume tumors to observe changes related to later stages of neuroepithelial interactions. It is well known that there is an increase in prostate cancer incidence with age. Previous publications have also suggested that changes in nerve area might be age related. Therefore, we selected patients with ages spanning three decades to be certain that our results would not be affected by age. Twenty patients were selected from an autopsy series as controls. Their prostates had been removed and processed similarly to those of the

patients with cancerous prostates and the absence of cancer confirmed histologically. Five patients from each of four groups categorized by age (decades) were selected so that nerve density could be compared with that of cancer patients within the same age group.

The radical prostatectomy specimens were grossed, fresh fixed in formalin, and paraffin-based tissue mounting medium to form whole-mount paraffin blocks. Sections (4 μm thick) were immunostained with antibody against the nervous protein S100 (DAKO) for 1 h at room temperature. A pathologist (G.E.A.) read all the immunostained whole-mount slides from each patient. Each slide was marked at points of the highest nerve concentration (hotspots) in each of the following regions: tumor, benign prostatic hyperplasia, high-grade prostatic intraepithelial neoplasia (HGPIN), anterior capsule, posterior capsule, neurovascular bundles, peripheral zone, transition zone, and seminal vesicles. Because the depth of the serial section was such that certain regions could not be observed in cross-section or because for any particular slide, there was insufficient nerve concentration to warrant mapping a hotspot; not every region had a hotspot on each slide. The net result of this was that each slide featured an average of ~3 of 9 possible hotspots.

A single individual digitally imaged the hotspot marked on the mapped slides using a Nikon microscope and an Ikegami digital camera. The images were analyzed using the Optimas 6 Image Analysis Suite and using the brown color of the positively staining nerves as a threshold; the cross-sectional area of the neural hotspots was calculated and entered into a database. A biostatistician performed statistical analysis of the nerve area calculations using SPSS software. Data were recorded for an experimental group (patients with prostate cancer) and a control group (patients without prostate cancer). The data were further subdivided by region of the prostate from which specimens were taken. *t* tests and Mann-Whitney tests were used to compare similar neural regions in experimental and control groups. Mann-Whitney tests were used to compare prostate cancer with peripheral zone and benign prostatic hyperplasia, and Wilcoxon signed rank tests were used to compare PIN versus prostate cancer and peripheral zone versus transition zone. Linear regressions were done to study the relationships between nerve area and age.

Axonogenesis in HGPIN. To determine whether axonogenesis was present in preneoplastic lesions, we used a tissue microarray built with tissues from 100 patients. Normal and HGPIN were represented twice per patient in 2 mm cores. Sections were stained with antibodies against PGP 9.5. The cores were digitized with the BLISS system at ×20 on the subepithelial plexi. The images in Fig. 6 (see Appendix) on the left show representative examples of normal prostate and HGPIN with the nerves of the subepithelial plexi staining in brown. The subepithelial neural density quantification was done with the Optimas 6 Image Analysis Suite.

Three-dimensional reconstruction of prostate. To establish the visibility of axonogenesis in three-dimensional studies or determine that it is only seen in two-dimensional studies, we used an entire prostate that was sectioned according to protocol and embedded in paraffin entirely in blocks. Each block was then sectioned on whole mounts using 5 μm sections. Alternate step sections were immunostained with antibodies against PGP 9.5 (Novacastra Laboratories) for a grand total a total of 400 whole-mount sections as follows: The slides were deparaffinized and hydrated through xylenes and graded alcohol series. Antigen retrieval was obtained by using steam heat in 10 mmol/L sodium citrate buffer (pH 6.00; Signet Laboratories) for 25 min followed by a 10-min cool down and a distilled water wash three times. The slides were endogenously blocked in 3% H_2O_2 (Fisher) for 5 min and avidin-biotin blocked using Vector Avidin/Biotin Blocking Kit. Primary antibody is applied for 1 h. The Vectastain Elite ABC Reagent is applied to the slides for 5 min. The peroxidase substrate is prepared and applied according to the kit instructions and chromogen (diaminobenzidine) was used for 6 to 10 min, counterstained in Mayer's hematoxylin (Poly Scientific) 2 min, dehydrated, cleared, and mounted.

PGP 9.5 is expressed almost exclusively by nerves. The tumors were demarcated on each slide and the slides were scanned at high resolution. The images were then reconstructed three-dimensionally using specially created algorithms and software (Amerra). Rendering of the composite images has been a limiting factor in this endeavor, as constructing an image with 50 sections requires 1 week of continuous computer time. For the surface plot of the nerve area, we used image conversion from ImageJ, version 1.37, NIH.

Ganglia and neurons. Using the same set of patients as those in the nerve study, we examined the status of intraprostatic and extraprostatic neural ganglia. Based on the histology, slides from 17 of 20 normal patients and 23 of 27 prostate cancer patients were qualified for further analysis. Slides were disqualified if they had no, or incomplete, neurovascular bundle. S100 stained all neural tissues including ganglion cells. Ganglion cells were easily identified visually. A single pathologist identified and measured ganglia in each whole-mount section of 50 entire radical prostatectomies. We selected as the one representative slide for each patient the slide that held the most ganglia. We counted neurons in all ganglia of the neurovascular bundle. Each neurovascular bundle had 1 to 5 ganglia. The total number of neurons per case and the average number of neurons per ganglion per case were used for comparison.

Proliferation in human tissues. The proliferation rates of nerve cells and neurons in human tissues were determined using the immunoperoxidase method with antibodies against Ki-67 (Santa Cruz Biotechnology). The slides were deparaffinized and rehydrated in graded ethanol, and antigens were retrieved using steam in 10 mmol/L citrate buffer (pH 6.0) for 30 min. The slides subsequently were blocked with blocking protein (DAKO) for 10 min, then incubated with the polyclonal antibody Ki-67 (C-20), for 1 h at room temperature at a dilution of 1:50 followed by the secondary biotinylated antibody applied for 30 min and 30 min of incubation with streptavidin peroxidase (DAKO LSAB + HRP kit). After rinsing, slides were visualized by diaminobenzidine chromogen solution (DAKO) and counterstained with routine hematoxylin. Positive staining of Ki-67 is nuclear.

Tissue microarray analysis. Radical prostatectomy specimens were process using whole-mount slides. The clinical and pathologic data of these patients were available for analysis in the Baylor Prostate Specialized Program of Research Excellence data bank. The tissue microarrays were built using a manual tissue arrayer (Beecher Instruments). A cohort of 100 patients was selected, 50 with biochemical recurrence (defined as a prostate-specific antigen > 0.4 ng or 2 consecutive rises or clinical recurrence) and 50 patients without recurrence. This cohort has overrepresentation of the recurrence group and is not meant as a longitudinal cohort designed to study biomarker potential rather the clinical implications of a biological process. Triplicate 0.6 mm cores were obtained from the areas of the tumor. Slides were stained with PGP 9.5 as described above. Tissue slices were reviewed and imaged using the Nuance image deconvolution system. Image analysis was done using internal algorithms measuring area of stain.

Cloning of S4F. Primers were designed according to S4F sequence (GenBank accession no. NM-004263) to isolate S4F cDNA by real-time PCR: forward 5′-GCGAATTCCAGAGGCCGTAGCTTGCG (contain an *Eco*RI site) and reverse 5′-GCGAATTCTCACTCCGTTCCAGTGATC (contain an *Eco*RI site). Total RNA was extracted from DU145 human prostate cancer cell lines, and reverse transcription was done using SuperScript III First-Strand Synthesis System (Invitrogen). The S4F expression vector pEGFP-S4F was constructed by inserting S4F cDNA into pEGFP-C1 *Eco*RI site (Clontech).

Generation of S4F retrovirus. The retroviral expression system was developed in Dr. Garry Nolan's laboratory. Retroviral vector pBMN-I-GFP was purchased from Addgene and retroviral packaging cell line Phoenix-A was obtained from the American Type Culture Collection safe deposit. To generate pBMN-I-GFP-4F, S4F cDNA was first inserted into pBMN-I-GFP *Eco*RI site, and a HA tag with NH_2-terminal S4F cDNA obtained by real-time PCR was inserted into *Bam*HI site (S4F NH_2-terminal region has a *Bam*HI site): forward primer 5′-CCGGATCCATGTACCCATACGACGTCCCAGACTACGCTCCAAA-GATGCCGGCCTCTG (contain a *Bam*HI site) and reverse primer

5′-CCAACATAAAGTGTGTGG. Max Efficiency stbl2 Competent cells (Invitrogen) were used to produce pBMN-I-GFP-4F plasmid. pBMN-I-GFP-4F was then transfected into Phoenix-A cells by Calcium Phosphate Transfection kit (Invitrogen) according to Dr. Garry Nolan's laboratory protocol.[5] Retrovirus-containing medium was harvested 48 and 72 h post-transfection, filtered with 0.45 μm filter, and stored in -80°C.

Retroviral infection and expression of S4F. DU145 and LNCaP cells were planted in T25 flask at a density of 30% to 50%. The next day, cell growth medium was removed and 1 mL viral supernatant was mixed with 1 mL fresh cell growth medium containing 8 μg/mL polybrene (final concentration) and added to cells. Three hours later, cells were washed with PBS, and 5 mL fresh growth medium was added to cells. After 48 h, cells were separated. S4F expression was confirmed by Western blot (LNCaP cells) using anti-HA antibody (Abcam) or quantitative PCR (DU145 and LNCaP cells).

S4F small interfering RNA cell transfection. DU145 S4F pretransfected cells were plated in six-well plate at desired density with antibiotic-free DMEM containing 10% FBS 1 or 2 days before to reach 75% to 80% confluency for the small interfering RNA (siRNA) transfection experiment. Cells were incubated in a humidified incubator maintained at 37°C with 5% CO_2. SiGENOME siRNA to S4F (Dharmacon) and SiCONTROL Nontargeting Duplex siRNA (negative control; Dharmacon) for eliciting RNA interference were transfected separately into DU145 cells using DharmaFECT 1 transfection agent (Dharmacon) and Opti-MEM I (Invitrogen) with concentration at 110 nmol/L. Briefly, prepare the siRNA-lipid complexes for each siRNA reagent by combining Opti-MEM, DharmaFECT 1, and siRNA. Cells were incubated at 37°C in 5% CO_2 for 48 h and supernatant from S4F-siRNA-transfected experiment wells and the negative control wells were collected at the time, respectively. The S4F siRNA sense sequence was GUACUGAGGUGACACAAGUUU and the antisense sequence was 5′-PACUUGUGUCACCUCAGUACUU. The extent of target genes' silencing was evaluated by measuring mRNA copy number using quantitative real-time PCR.

Target gene knockdown level verified by real-time quantitative PCR. Total RNA was extracted at 48 h after siRNA transfection and purified using the RNAqueous-4PCR Kit (Ambion). First-strand synthesis was done using SuperScript III kit (Invitrogen). The expression level of target gene was determined for each experimental sample by quantitative PCR. The ABI Prism 7000 sequence detection system (Applied Biosystems) was used for quantitative PCR analysis using rRNA 18S as endogenous control. S4F and 18S genes were amplified using S4F and 18S primers and TaqMan probes (TaqMan gene expression assay; Applied Biosystems). A validation experiment was done using 1:10 diluted cDNA templates. The log input amount of cDNA versus ΔCt was generated to show that the efficiencies of the targets and references were approximately equal. Each sample was done in separate wells in duplicate. Reaction conditions include 12.5 μL of 2× TaqMan Universal Master Mix, 1.25 μL S4F target and 18S primers and probes mixture, 40 ng template cDNA from each sample, and nuclease-free water to a 96-well reaction plate. The total reaction volume is 25 μL. The TaqMan cycling conditions were as follows: 2 min at 52°C, 10 min at 95°C, and 42 cycles of 15 s at 95°C followed by 1 min at 60°C. Calculation was done using ΔCt values as the calibrator from Silencer Negative siRNA pretransfected DU145 cells. S4F probe sequence was 5′- CGCTTCCAATCTCTGAGGCTGACTC.

N1E-115 neurite assay. DU145 cells were infected or uninfected with S4F retrovirus in one T25 flask. After 48 h, cells were separated from 1 T25 flask to 6 T25 flask and grow in DMEM with 10% FBS. Four days later, supernatant was collected for N1E-115 neurite assay. Briefly, mouse neuroblastoma N1E-115 cells were induced by serum starvation for 24 h, and 1×10^4 cells were mixed with 1 mL supernatant and 1 mL serum-free DMEM (per well) and planted to six-well plate. Plates were incubated at 37°C and 10% CO_2 for 72 h. Then, each sample was photographed at locations of high neurite density and high cell density. Neurite length was computerized via Optimas 6 Image Analysis Suite; total number of cells and the number of cells with neurite sprouting were counted manually.

[5] http://www.stanford.edu/group/nolan/

Results

In vitro *neurogenesis assays.* To determine if soluble factors secreted by prostate cancer cells or from cocultures of prostate cancer cells with DRG could enhance neurogenesis and/or axonogenesis, we incubated supernatants from such cultures or control cultures with human or mouse neuroblastoma cell lines. For PC-12 cells, the neurite absorbance of samples grown in DU145/DRG supernatant was significantly higher than that of samples grown in supernatant from DU145 alone (0.357 versus 0.282; $P < 0.05$) and plain serum-free RPMI 1640 (0.357 versus 0.238; $P < 0.001$; Fig. 1A). Samples grown in supernatant of DU145 alone also had significantly higher absorbance than control RPMI samples ($P < 0.05$). We believe that the levels of DRG alone and DU145 alone are lower than the serum control because of nutrient consumption.

Similar results were obtained with mouse N1E-115 neuroblastoma cells. N1E-115 cells grown in DU145/DRG PNI coculture supernatant had significant increase in total length of neurite outgrowth (41.585 versus 15.3; $P = 0.0053$; Fig. 1B) as well as more neurite sprouting (0.082 versus 0.030; $P = 0.0282$) compared with cells grown in the supernatant of DRG alone group (Fig. 1C). However, there was no significantly higher percentage of cells displaying neurites in the coculture model than the DRG alone group. In summary, the neurites were longer and had more sprouting or branching. In contrast to the PC-12 cell experiment, a trend but no significant difference was identified between variables of N1E-115 cells grown in DU145/DRG PNI coculture supernatant compared with the DU145 cancer cell supernatant control.

Analysis of nerve density in human prostate tissues. Axonogenesis *in vivo* would lead to increased nerve density. To determine if nerve density is increased in human prostate cancer, we compared the nerve density of different areas of prostates without and with cancer. The nerve density in the neurovascular bundle of prostate cancer patients was significantly higher than that in patients without prostate cancer (182.56 versus 110.18; $P = 0.001$). More importantly, the nerve density within foci of prostate cancer was significantly higher than in the peripheral zone of patients either with cancer (46.52 versus 27.57; $P = 0.0145$) or without cancer (21.45; $P = 0.0002$; Fig. 2A). The nerve density in the peripheral zone of patients with and without cancer was not statistically different.

Previously, we identified a decline in nerve density tendency in the peripheral zone with increasing age (20). However, in prostates with cancer, this relationship/tendency is lost, and we can see a trend of increased nerve density with age (Fig. 2B). It is important to stress that the peripheral zone is the area where most prostate tumors develop. There is also no relation between age and nerve density within tumors. In conjunction, these results suggest that cancer-related axonogenesis might have a field effect over the entire prostate, as the increase in nerve density can also be found in nonneoplastic tissues. However, this effect is not sufficiently evident, as we were not able to detect significant differences between the peripheral zone of patients with and without cancer.

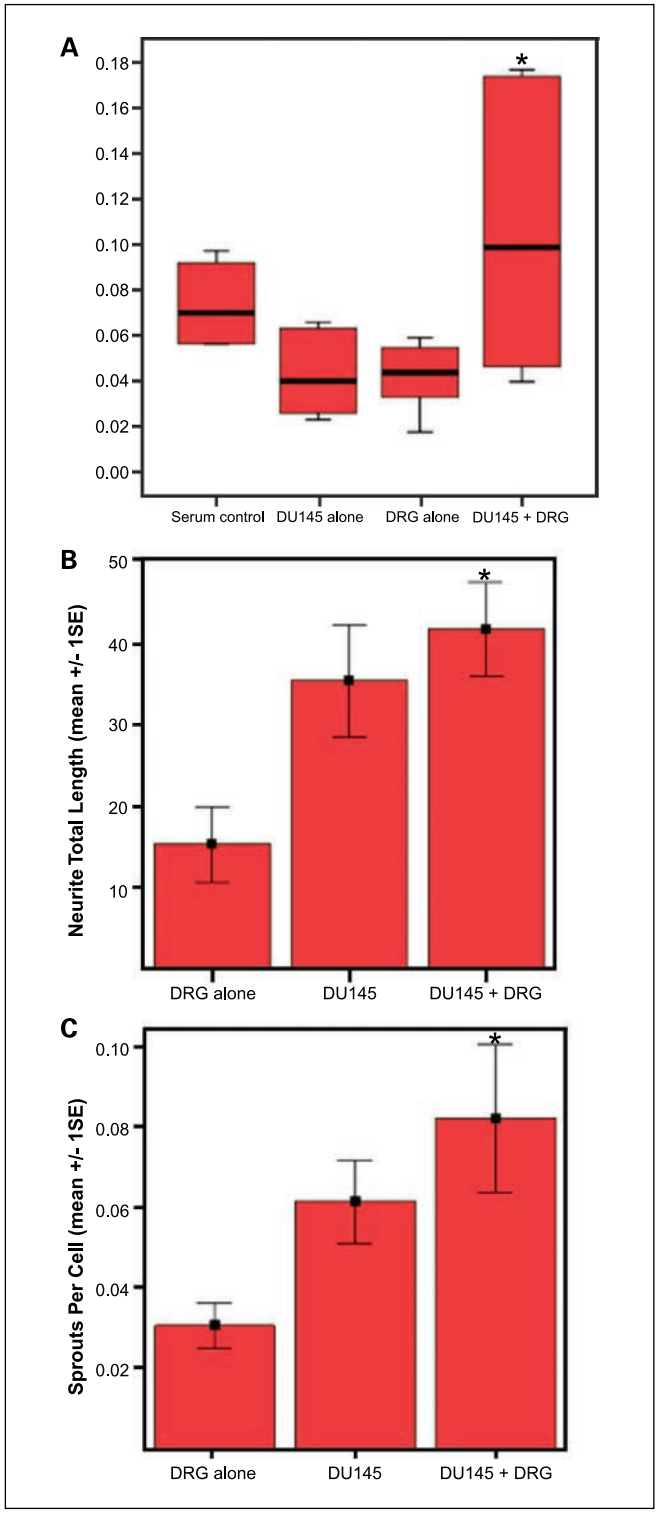

Fig. 1. *A,* neurite absorbance of PC-12 samples grown in DU145/DRG supernatant was significantly higher than that of samples grown in supernatant from DRG alone, DU145 alone, and plain serum-free RPMI. *B* and *C,* N1E-115 cells grown in DU145/DRG PNI coculture supernatant had significant increase in total length of neurite outgrowth as well as more neurite sprouting compared with cells grown in the supernatant of DRG alone group but not the DU145 alone. Box plots were used for nonparametric data and show the median (*line*), interquartile range (the box includes the middle 50% of observations), and whiskers extending out to the farthest points that are not outliners. These plots allow the reader to visually compare distributions of the variables. Bar graphs used for normal data show the mean ± 1 SD. *, statistical significance at 95% confidence interval.

The preneoplastic lesion in the prostate is HGPIN. The mean nerve density in normal prostatic glands was 0.404 (median, 0.0360), whereas the mean nerve density in HGPIN was 0.615 (median, 0.574; P = 0.000; n = 38; Fig. 2C). Matched pair analysis was also significant (P = 0.000). These data suggest that axonogenesis is already present in preneoplastic lesions of the prostate and is probably an early event in initiation or supports the initiation of prostate cancer.

To confirm these results, we performed two-dimensional reconstructions of whole-mount sections stained with antibodies against S100. This required manually taking pictures of entire whole-mount slides at ×200 and reconstructing the images into one final image. Through color substitution and negative images, we can clearly note that most of the nerves are located in the periphery of the prostate (nerves in green; Fig. 3A). More importantly, the prostate with cancer (Fig. 3B) has a substantial increase in nerve density (44,474) units measured by ImageJ version 1.37, NIH compared with the prostate without cancer (19,100; Fig. 3C).

Three-dimensional reconstruction was needed to show that axonogenesis is not a two-dimensional artifact. Figure 4A show a whole-mount slice stack of the prostate showing the acinar architecture. Figure 4B shows the nerves in green identified with antibodies against PGP 9.5 in individual whole-mount sections. These were reconstructed three-dimensionally.

Figure 3D is a reconstruction of the 400 sections of the prostate in different perspectives. The amount of information in this model does not permit visualization of the nerves. Subsequently, Fig. 3E shows the entire prostate broken into sections of ~50 slides. The blue areas represent prostate parenchyma and the empty circle areas from which frozen tissues were obtained for tissue banking. Figure 4D is a closer view of the first stack showing only the prostatic parenchyma. The nerves are marked with dark brown in Fig. 4 E and F and the latter also shows the tumor in tan. Note that the tumor breaks the symmetry in the distribution of nerves in the prostate, with most of the nerves and the largest nerves on the left side of the image, where the tumor is located. This is better represented using a surface plot of the nerve area where the area and intensity of stain are represented in the *Y* axis of the plot (Fig. 4C; ImageJ, version 1.37, NIH). Image analysis with Image J corroborated the asymmetry, where the left half of the image has 14,235 units, whereas the right has 6,205 units. An animated version of Fig. 4D to F can be found in Supplementary Data.

Analysis of ganglia size and neuron number in prostates. To address the question of cancer-related neurogenesis, we analyzed ganglia size and neuron numbers in prostates. Ganglia in the prostate are well-described and recognizable anatomic structures in the prostate. The total area of ganglia in each radical prostatectomy was higher in patients with prostate cancer than in those without cancer (161.4 versus 83.5 mm; P = 0.001). The average size of each ganglion was also larger in the patients with prostate cancer (6.8 versus 4.9 mm; P = 0.000). These data suggest that it is possible that not only the axons but also the neurons are involved in the process of axonogenesis/neurogenesis. To determine if the number of neurons was increased in prostate cancer, we counted the number of neurons within each prostatic ganglia. Neurons are easily recognized morphologically in the ganglia due to their histologic structure and size. The total number of neurons in all ganglia of patients with cancer was higher than in those without

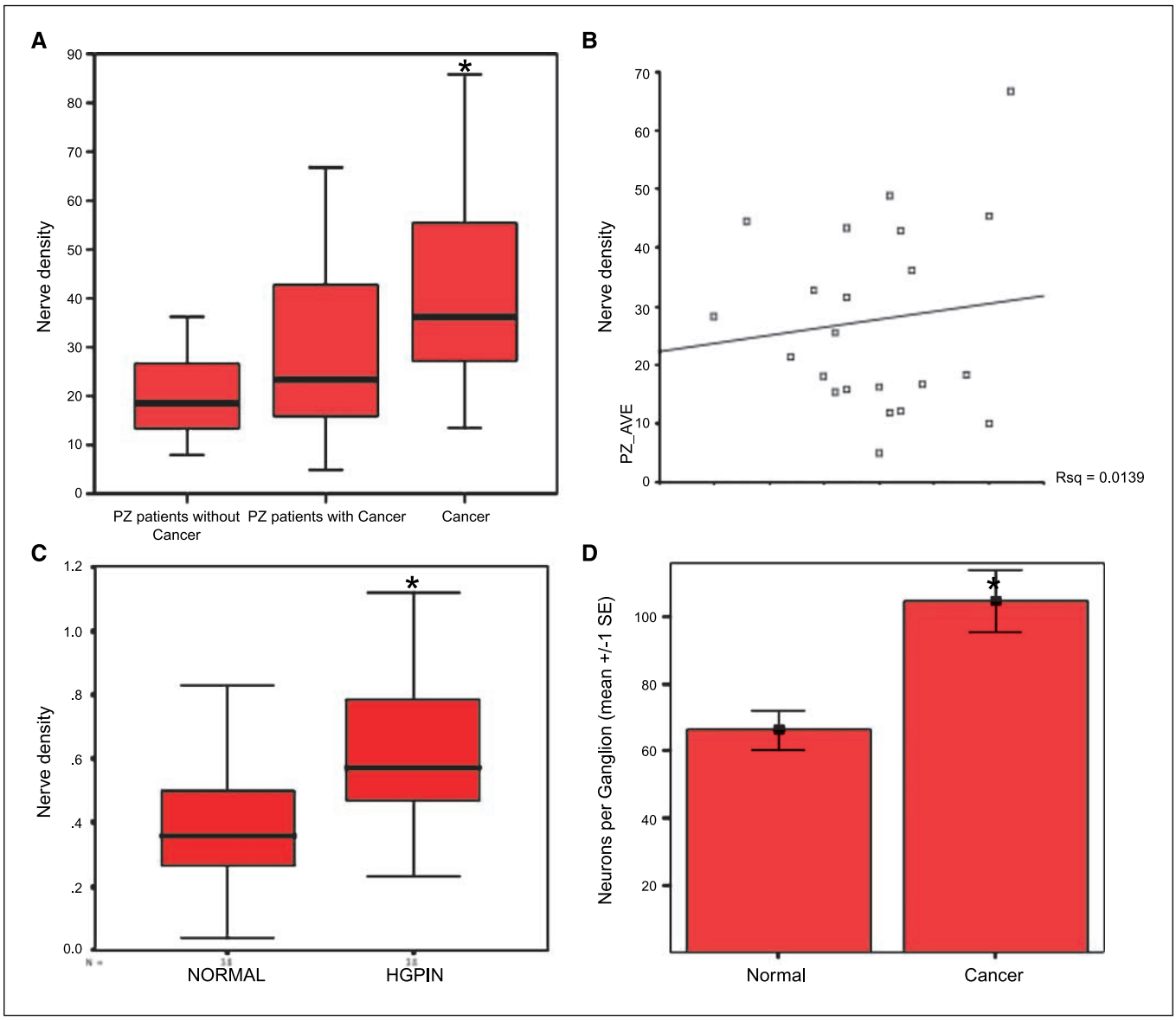

Fig. 2. *A,* nerve density in the prostate cancer areas is greater than the peripheral zone of patients with cancer and without cancer. The latter two are not statistically significant. *B,* nerve density tends to increase with age in the unaffected peripheral zone of patients with cancer. *C,* nerve density is increased in the subepithelial plexi surrounding HGPIN compared with the matched unaffected peripheral zone area from the same patient. *D,* number of neurons per ganglia in increased in patients with cancer than patients without cancer. Box plots were used for nonparametric data and show the median (*line*), interquartile range (the box includes the middle 50% of observations), and whiskers extending out to the farthest points that are not outliners. These plots allow the reader to visually compare distributions of the variables. Bar graphs used for normal data show the mean ± 1 SD. *, statistical significance at 95% confidence interval.

cancer (mean, 271; median, 270 versus mean, 188; median, 166; P = 0.001). Similarly, individual ganglion of patients with cancer had a mean of 104.70 neurons, whereas patients without cancer had a mean of 66.41 neurons (P = 0.001; Fig. 2D). We did not see a difference in the number of ganglia related to age in prostates of either patients with or without cancer. To test whether neurons were dividing, we immunostained the PNI microarray with Ki-67. We were unable to identify any positive nuclear staining in neurons within ganglia. Occasional Schwann cells were positive, indicating proliferation. In summary, prostate cancer was associated with increased numbers of neurons within prostatic ganglia.

Clinical significance of axonogenesis and neurogenesis. Using Spearman tests, we identified a correlation between the area of PGP 9.5 (nerves) and extracapsular extension, a measure of spread of the prostate cancer beyond the prostate and aggressive disease. The correlation coefficient was 0.470 and P = 0.0272 (Fig. 5A). Increased numbers of neurons were associated with seminal vesicle invasion (data not shown). More importantly, the median area of PGP 9.5 stain was 279 in the nonrecurrence group versus 615 in the group of patients with recurrence (Fig. 5B). These data strongly suggest that axonogenesis is functionally significant in human prostate cancer disease and is involved in the progression of prostate cancer to aggressive and recurring disease.

S4F is overexpressed in the PNI* in vitro *model. Gene profiling studies were done previously on the PNI coculture [DU145 (prostate cancer) and control cells]. A 2-fold cutoff was

used to identify genes that were significantly elevated in the PNI coculture than cancer cells growing alone. Numerous genes relating to neurogenesis were identified in the cancer cells growing in the presence of nerves. Among these, we selected those that were related to neurogenesis. We identified S4F as the one potentially most significant biologically. Using quantitative PCR, the S4F gene was overexpressed in the DU145/DRG coculture samples relative to DU145 alone control by 1.244 on day 2 and 2.031 on day 14, confirming the cDNA array data.

S4F overexpression. By transient transfection, we detected S4F expression in LNCaP cells. However, in stable LNCaP cells, Western blotting shows that the GFP-4F protein is not expressed at the full length (~112 kDa) as shown in transient transfection, suggesting a different packaging of the protein or cleavage. After cloning S4F, we inserted a HA-tagged S4F into a retroviral vector pBMN-I-GFP. Both cell lines, LNCaP and DU145, were infected with S4F retrovirus, confirmed by GFP expression in the cells (day 6; Fig. 6A). Using quantitative PCR, we detected S4F expression in both LNCaP (400-fold) and DU145 (40-fold) cells, however, at different amplification levels (day 7). Protein expression was identified using antibodies against the HA tag in Western blots (LNCaP, day 6; Fig. 6B). S4F was also identified in the supernatant, although inconsistently. We were not able to detect it in DU145 cells, which we believe is related to the low sensitivity of the HA antibody.

Influence of S4F on N1E-115 neurogenesis assay. For the neurogenesis assays, we selected the DU145 cells. In our experience with the PNI *in vitro* model, the DU145 cells are more suitable for inducing neurogenesis than LNCaP cells. Experiments with the supernatant obtained from the DU145 cells infected with S4F retrovirus (DU145/S4F) showed an induction in neurogenesis in the N1E-115 neurite assay. At

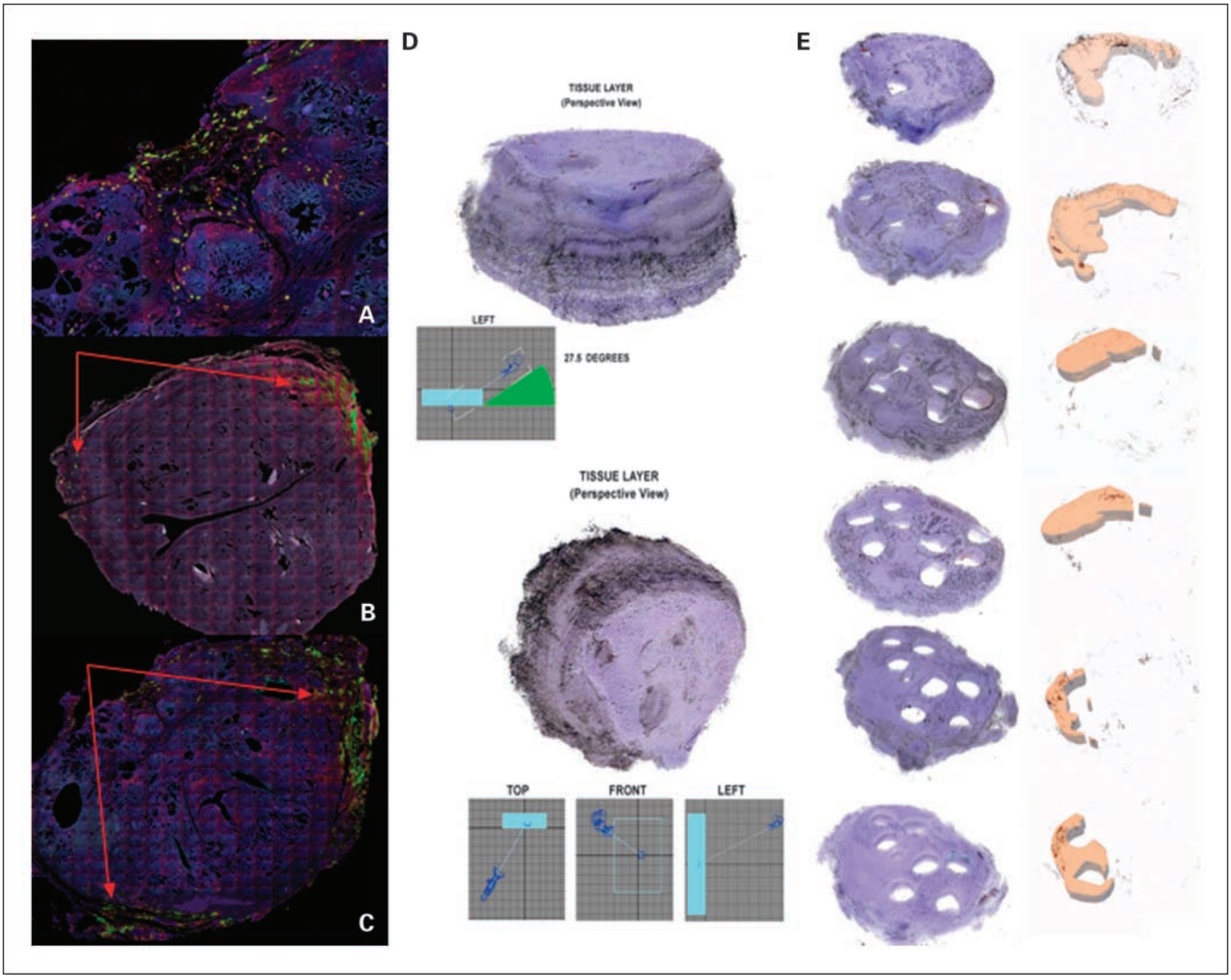

Fig. 3. *A,* two-dimensional reconstructions of whole-mount sections stained with antibodies against S100. This required manually taking pictures of entire whole-mount slides at ×200 and reconstructing the images into one final image. Through color substitution and negative images, we can clearly note that most of the nerves are located in the periphery of the prostate (nerves in green). *B,* nerves in green are seen in this two-dimensional reconstruction of a patient without cancer in its entire prostate. *C,* prostate with cancer has a substantial increase in nerve density (green areas in the periphery of the prostate) compared with the prostate without cancer (*red arrows*). *D,* three-dimensional stacking of ~400 whole-mount sections yields images seen at different angles. Because these composite images contain too much information, there is blurring of distinct anatomic structures and loss of individualization of nerves. *E,* three-dimensional stacks of ~50 whole-mount sections with the prostate parenchyma seen in the left and the tumor (*light tan*) and the nerves (*dark brown*) on the right. Note that the nerves are more prominent on the side with the prostate cancer tumor. *Blue areas,* prostate parenchyma and the empty circle areas from which frozen tissues were obtained in this specimen.

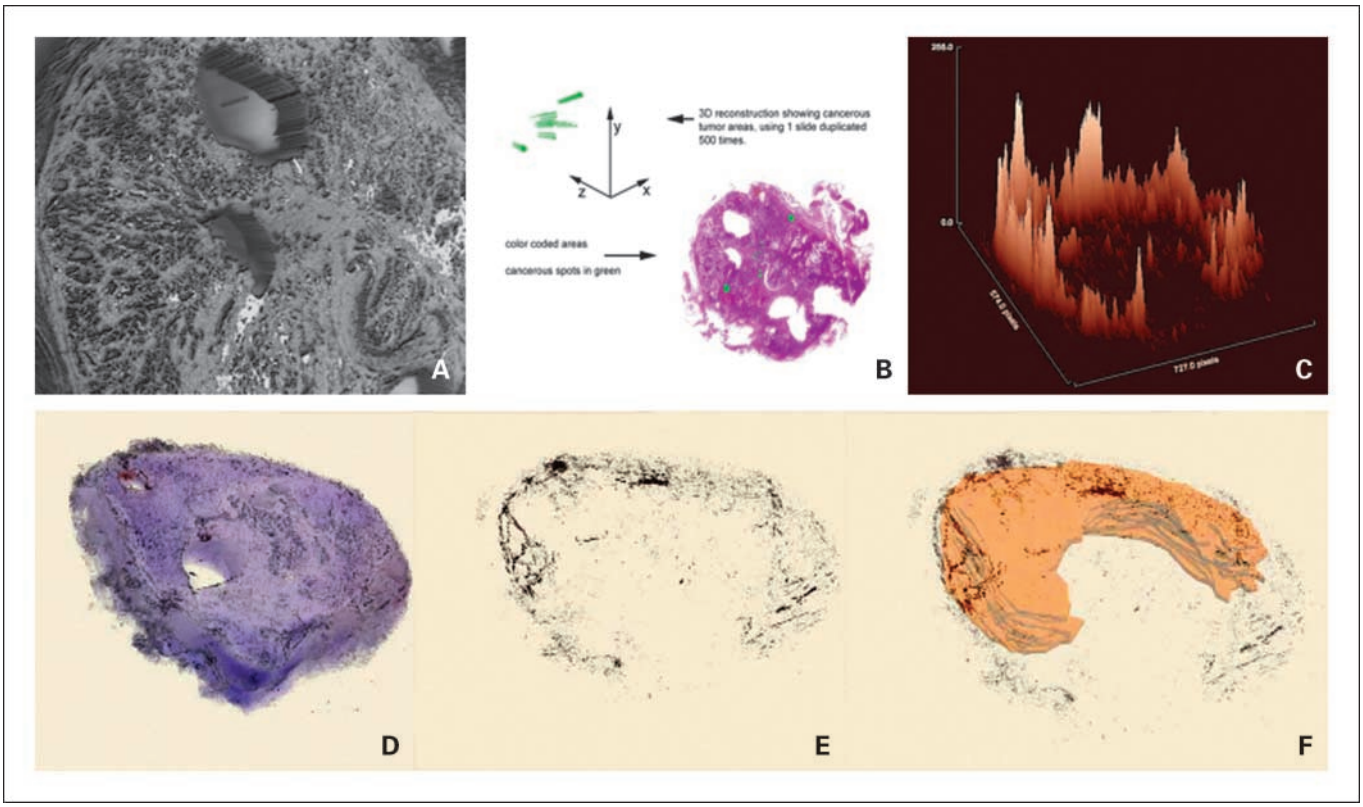

Fig. 4. *A,* three-dimensional reconstruction of a whole-mount slice stack of the prostate showing the acinar architecture. *B,* whole-mount slides were immunostained with antibodies to PGP 9.5 to mark the nerves. *C,* nerves in green identified with antibodies against PGP 9.5 in individual whole-mount sections. These were then reconstructed three-dimensionally. *C,* surface plot of *E. Y axis,* area and intensity of stain. Note the asymmetry between the left and the right sides of the image, with most of the tallest bars on the left. *D* to *F,* three-dimensional reconstruction of the first 50 apical slides of the radical prostatectomy. *D,* closer view of the first stack showing only the prostatic parenchyma. *Blue areas,* prostate parenchyma and the empty circle areas from which frozen tissues were obtained in this specimen. The nerves are marked with dark brown in *E* and *F* and the latter also shows the tumor in tan, and *F* adds the tumor and superimposes it to the nervature. Note that the tumor breaks the symmetry in the distribution of nerves in the prostate, with most of the nerves and the largest nerves on the left side of the image, where the tumor is located.

72 h, we observed a 2-fold increase in the number of N1E-115 cells that were sprouting neurites (22.1% versus 10.7%; $P < 0.002$; Fig. 6C) and also a >2-fold increase in the average length of the neurites compared with empty vector controls (4.4 versus 2; $P < 0.0001$; Fig. 6D). No significant induction of neurogenesis was observed with the supernatant derived from the empty vector cells and the naive DU145 cells. We obtained similar results with supernatant from LNCaP S4F retrovirus-infected cells (data not shown).

Subsequently, DU145/S4F cells were transfected with S4F siRNA. Forty-eight hours after siRNA transfection, S4F gene expression levels in DU145 cells were knocked down by 79% compared with negative control scrambled siRNA-transfected DU145 cells. Supernatant from these cells was then used in a N1E-115 neurogenesis assay. We observed a significant decrease in the number of cells sprouting neurites against the scrambled siRNA controls (12% versus 6.9%; $P < 0.0002$). The average length of the neurites also decreased significantly (1.9 versus 1.47; $P < 0.01$). No differences were found between the naive DU145/S4F cells and the scrambled controls (Fig. 6E and F).

Discussion

We hereby introduce a novel biological phenomenon, cancer-related neurogenesis and axonogenesis. Our *in vitro* experimental and human prostate tissue data show the existence of cancer-related axonogenesis/neurogenesis. We also present data substantiating its involvement and significance in aggressive human prostate cancer and a putative regulatory mechanism based on S4F.

Neuroepithelial interactions occur at several stages of oncogenesis and through several mechanisms. PNI is the most obvious and best known; in fact, PNI has been recognized for >100 years. However, biological studies that address interactions between cancer and nerves such as PNI only began to recently appear (10). PNI provides growth and survival advantage for prostate cancer cells in the perineural space. The perineural space conceivably permits selection pressures associated with increased metastatic potential. It is probable that PNI is preceded by axonogenesis/neurogenesis in initial stages of preneoplastic lesions (PIN) and subsequent carcinogenic stages. Axonogenesis most likely facilitates PNI, which would then become the second step of neuroepithelial interactions in prostate cancer. Therefore, understanding the specific mechanisms of carcinoma/nerve interactions in neurogenesis is key to developing cancer-related therapies.

Interaction between nerves and epithelial cells are not exclusive to the realm of cancer. Nerves, stromal cells, and epithelia have numerous interactions during development and in response to injury. Nerves are involved in the regulation of embryologic development and tissue repair process. The nervous system is first to be formed during embryonic

development and subsequently regulates the development of dermatomes and somatomes. Concordantly, the formation of the mouse pelvic floor is dependent on the survival of a nucleus in the lower spinal cord (21). In the absence of androgens, this nucleus involutes and the embryo acquires the default female phenotype. In the presence of androgens, the nucleus remains and regulates the formation of the pelvic floor. This dependence on neural regulation results in an organ that is very rich in nerves and neural growth factor (22). In conjunction, these facts provide a logical framework by which prostate cancer and other cancers might use strong embryologic and wound repair mechanisms such as neural control of epithelial growth to progress.

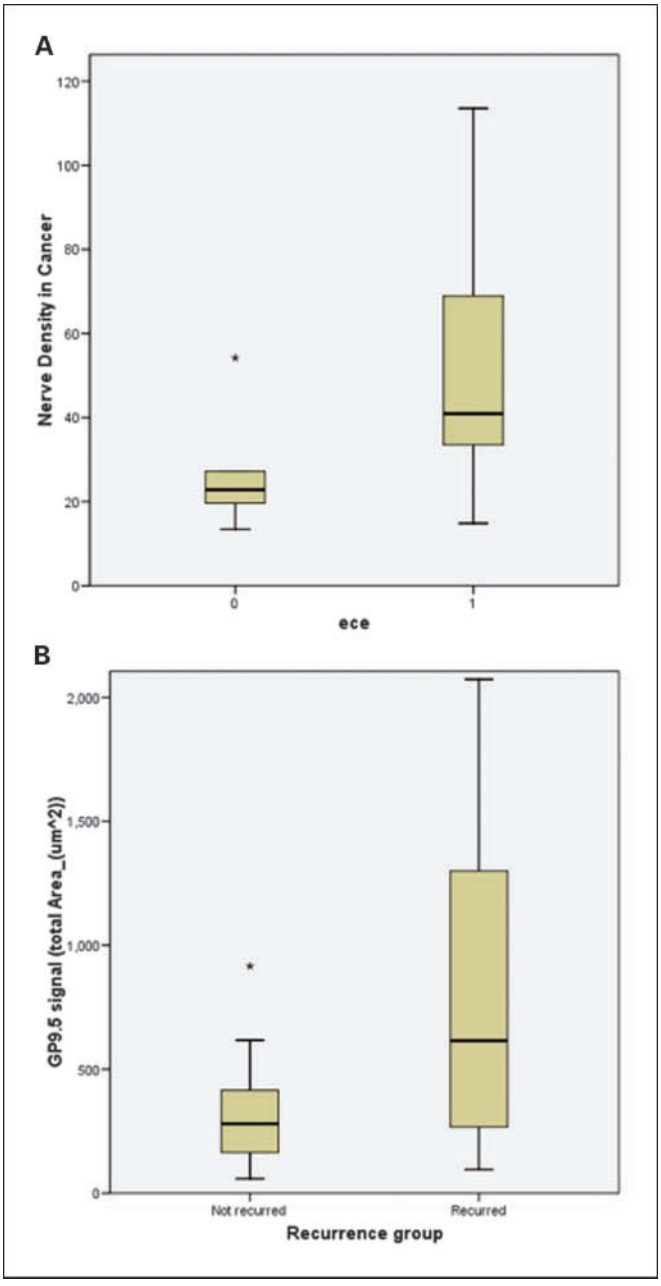

Fig. 5. *A,* patients with extracapsular extension of their prostate cancer (*1*) have a higher nerve density in their tumors that those without extracapsular extension (*0*). *B,* prostates of patients that have had prostate cancer recurrence have a higher tumor nerve density than those that did not recur, showing the functional significance of neurogenesis in human prostate cancer. Box plots were used for nonparametric data and show the median (*line*), interquartile range (the box includes the middle 50% of observations), and whiskers extending out to the farthest points that are not outliners. These plots allow the reader to visually compare distributions of the variables. Bar graphs used for normal data show the mean ± 1 SD. *, statistical significance at 95% confidence interval.

Our study presents cancer-related neurogenesis in prostate cancer and, to our knowledge, is the only study of this novel process. However, the process of cancer-related neurogenesis is not limited to prostate cancer but could also be significant in other cancers (data not shown). This process will likely have variable significance in various cancer types. Interaction between nerves and prostate cancer such as PNI are more readily evaluable in ''neurotropic carcinomas'' (prostate, pancreas, and head and neck tumors). This does not eliminate neurogenesis/axonogenesis as elements involved in carcinogenesis and progression of other tumor types. Future studies that specifically address other tumor types will help elucidate the universality of this novel phenomenon.

We have shown a spatial (three-dimensional) and temporal association between nerves and cancer *in vitro* and in human prostate tissues. Axonogenesis begins early and is found associated with HGPIN. However, the functional significance of axonogenesis/neurogenesis in preneoplastic lesions and prostate cancer progression needs to be clearly established. Is axonogenesis/neurogenesis a phenomenon coincidental to cancer development and progression, or is it necessary for carcinogenesis and progression? Our data strongly suggest that axonogenesis and neurogenesis are functionally significant in human disease and involved in the progression of prostate cancer to aggressive and recurring disease. Further functional denervation studies in transgenic mice will help elucidate this issue.

We show that the number of neurons per ganglia increased in prostate cancer patients compared with controls. In the future, we will investigate the origin of cancer-related neoneurons with two possible alternatives. The first is that neurons within ganglia are dividing and promoting rise to new neurons (neuronal neurogenesis). We have not been able to detect proliferation in human tissues. Another more realistic alternative is that stem cells give rise to cells that differentiate into neurons (stem cell neurogenesis). We believe that this is a more realistic alternative, as we have identified no data to suggest that neuronal division is occurring in humans. In humans, it is apparent that a population of cells in the central nervous system has the potential to derive neoneurons. One of the first descriptions of human neurogenesis came from cancer patients. Patients terminally ill with head and neck carcinomas were given bromodeoxyuridine and their brains were examined after death. Positively stained neoneurons were identified in the hippocampus (23). Of note is that head and neck carcinomas are neurotropic and not uncommonly tracked through the nerves up into the central nervous system. It is possible that the neurogenesis detected in this study was cancer-related neoneurons.

This study also proposes that S4F is involved in cancer-related axonogenesis/neurogenesis. Overexpression of S4F in cancer cells leads to increased neurogenesis in modified neurons and reduction of S4F levels in the same cells consequently reduces neurogenesis. We are perceptive that these data show only that S4F is sufficient but not necessary for cancer-related neurogenesis. In fact, as is common in other biological phenomena, redundant mechanisms will likely take over in the absence of S4F. The obvious candidates are other members of the semaphorin family. We do not exclude that

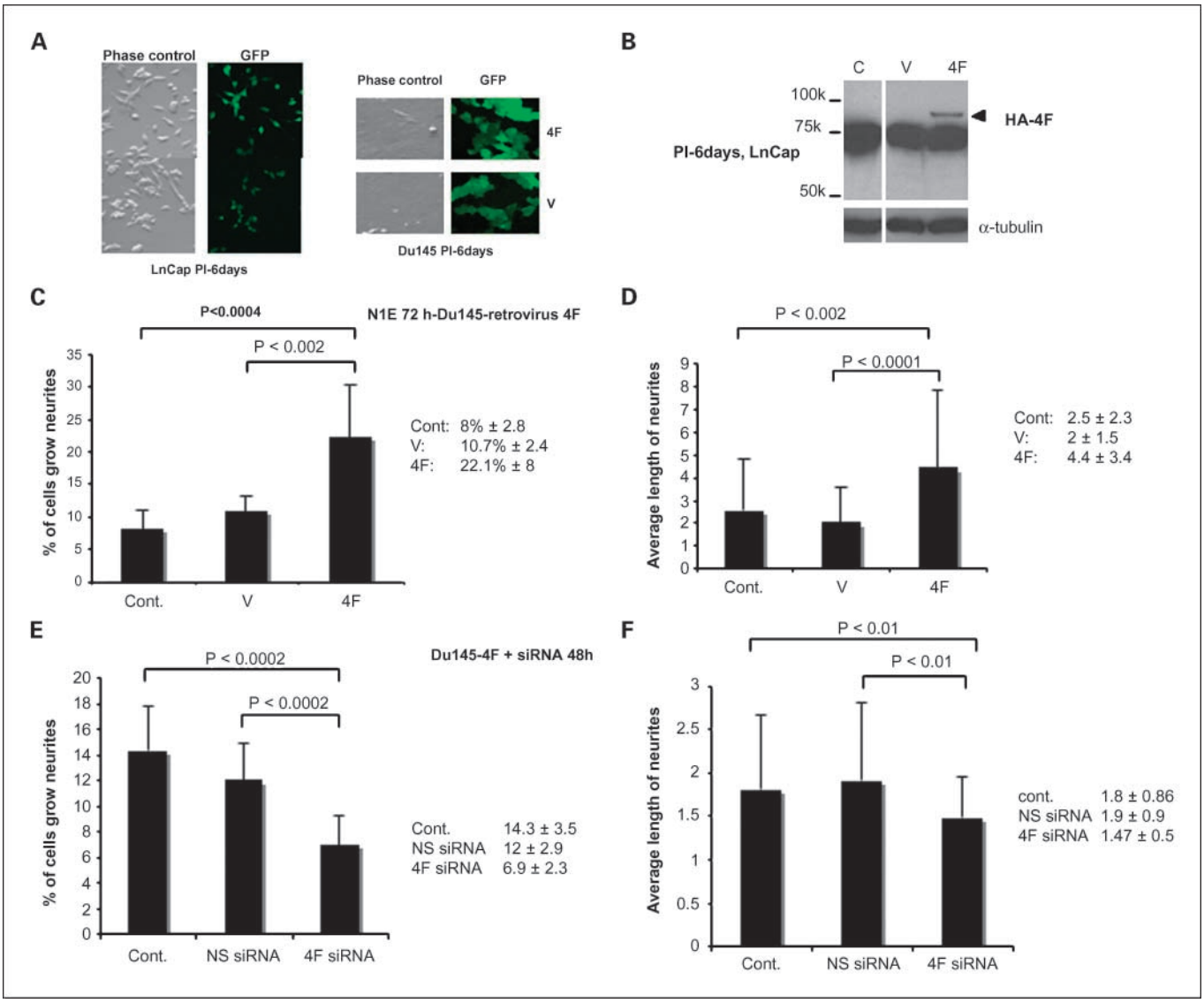

Fig. 6. *A,* GFP expression indicating that cells were infected by empty vector (*v*) or S4F retrovirus. *B,* Western blots showing HA-tagged S4F expression in LNCaP cells. Note that empty vector controls (*V*) do not produce S4F. *C* and *D,* N1E-115 neurite assay. An increase in the percentage of N1E-115 cells sprouting neurites and in the average neurite length is noted in S4F overexpressed cells compared with empty vector controls. *E* and *F,* decreased S4F expression by S4F siRNA transfection resulted in decrease of percentage of N1E-115 cells sprouting neurites and a decrease in the average neurite length compared with scrambled control (*NSsiRNA*).

other neurogenesis-related molecules might be involved and we are currently exploring other pathways.

Little is known about the biology of S4F. The structure of this transmembrane protein suggests that it could potentially be secreted. In our studies, we have identified, albeit inconsistently, S4F in the supernatant. We are, however, limited by the low detection threshold of the HA antibody and the lack of a S4F antibody. It is also possible that we are detecting S4F that is shed from dead cells. Future S4F protein structure research will help elucidate this issue. However, we are emboldened by the fact that our overexpression and underexpression studies using supernatant have direct influence on neurogenesis assays. Future studies will also address if S4F downstream secreted factors are more directly liked to cancer related neurogenesis.

A critical question remains. Does cancer develop in patients with predisposing higher nerve density? Although this is a possibility, our data indicate that this is unlikely. We did not identify significant differences in nerve density between the peripheral zones of patients with and without cancers. We did find increased nerve density in preneoplastic lesions compared with normal peripheral zone. Furthermore, the asymmetry in nerve density found in tumors compared with normal peripheral zone and the *in vitro* data strongly suggest that cancer cells induce neurogenesis. Finally, PNI seems to enhance the ability of prostate cancer cells to induce neurogenesis even further. Cancer-related neurogenesis is a new concept that requires further exploration. The origin of this phenomenon and the full spectrum of its functional involvement in carcinogenesis and progression will be addressed in future studies.

Disclosure of Potential Conflicts of Interest

No potential conflicts of interest were disclosed.

References

1. Villers A, McNeal JE, Redwine EA, Freiha FS, Stamey TA. The role of perineural space invasion in the local spread of prostatic adenocarcinoma. J Urol 1989; 142:763–8.

2. Doggweiler R, Zermann DH, Ishigooka M, Schmidt RA. Botox-induced prostatic involution. Prostate 1998;37:44–50.

3. Lujan M, Paez A, Llanes L, Angulo J, Berenguer A. Role of autonomic innervation in rat prostatic structure maintenance: a morphometric analysis. J Urol 1998; 160:1919–23.

4. Kato T, Watanabe H, Shima M, Kaiho H. Studies on the innervation of prostate. II. Histological changes of the dog prostate after transsection of its innervating nerves. Nippon Hinyokika Gakkai Zasshi 1971;62: 704–7.

5. Watanabe H, Kato H, Kato T, Morita M, Takahashi H. Studies on the innervation of the prostate. I. Tissue respiration of the dog prostate after the cutting off of the various innervating nerves. Nippon Hinyokika Gakkai Zasshi 1967;58:381–5.

6. Watanabe H, Shima M, Kojima M, Ohe H. Dynamic study of nervous control on prostatic contraction and fluid excretion in the dog. J Urol 1988;140:1567–70.

7. Martinez-Pineiro L, Dahiya R, Nunes LL, Tanagho EA, Schmidt RA. Pelvic plexus denervation in rats causes morphologic and functional changes of the prostate. J Urol 1993;150:215–8.

8. Wang JM, McKenna KE, McVary KT, Lee C. Requirement of innervation for maintenance of structural and functional integrity in the rat prostate. Biol Reprod 1991;44:1171–6.

9. Ernst P. Uber das Wachstum und die Verbreitung Bostariger eshwulste insbesondere des Krebes in den Lymphbahnen der Nerven. Beitr Pathol Anat 1905;7: 29.

10. Ayala GE, Wheeler TM, Shine HD, et al. *In vitro* dorsal root ganglia and human prostate cell line interaction: redefining perineural invasion in prostate cancer. Prostate 2001;49:213–23.

11. Ayala GE, Dai H, Ittmann M, et al. Growth and survival mechanisms associated with perineural invasion in prostate cancer. Cancer Res 2004;64: 6082–90.

12. Frisbie JH, Binard J. Low prevalence of prostatic cancer among myelopathy patients. J Am Paraplegia Soc 1994;17:148–9.

13. Frisbie JH. Cancer of the prostate in myelopathy patients: lower risk with higher levels of paralysis. J Spinal Cord Med 2001;24:92–4; discussion 5.

14. Tamagnone L, Comoglio PM. To move or not to move? Semaphorin signalling in cell migration. EMBO Rep 2004;5:356–61.

15. Scheiffele P. Cell-cell signaling during synapse formation in the CNS. Annu Rev Neurosci 2003;26: 485–508.

16. de Wit J, Verhaagen J. Role of semaphorins in the adult nervous system. Prog Neurobiol 2003;71:249–67.

17. Kumanogoh A. Involvement of immune semaphorins in the immune system. Tanpakushitsu Kakusan Koso 2002;47:2254–60.

18. Christensen CR, Klingelhofer J, Tarabykina S, Hulgaard EF, Kramerov D, Lukanidin E. Transcription of a novel mouse semaphorin gene, M-semaH, correlates with the metastatic ability of mouse tumor cell lines. Cancer Res 1998;58:1238–44.

19. Yamada T, Endo R, Gotoh M, Hirohashi S. Identification of semaphorin E as a non-MDR drug resistance gene of human cancers. Proc Natl Acad Sci U S A 1997;94:14713–8.

20. Powell MS, Li R, Dai H, Sayeeduddin M, Wheeler TM, Ayala GE. Neuroanatomy of the normal prostate. Prostate 2005;65:52–7.

21. Bitoh Y, Shimotake T, Sasaki Y, Iwai N. Development of the pelvic floor muscles of murine embryos with anorectal malformations. J Pediatr Surg 2002;37: 224–7.

22. MacGrogan D, Saint-Andre JP, Dicou E. Expression of nerve growth factor and nerve growth factor receptor genes in human tissues and in prostatic adenocarcinoma cell lines. J Neurochem 1992;59:1381–91.

23. Eriksson PS, Perfilieva E, Bjork-Eriksson T, et al. Neurogenesis in the adult human hippocampus. Nat Med 1998;4:1313–7.